

SATELLITES—NEW GLOBAL OBSERVING TECHNIQUES FOR ICE AND SNOW

By P. GLOERSEN and V. V. SALOMONSON

(Applications Directorate, Goddard Space Flight Center, Greenbelt, Maryland 20771, U.S.A.)

ABSTRACT. Starting with the TIROS-2 weather satellite in 1961 which permitted synoptic viewing of large-scale areas with an on-board television camera system, the capabilities of satellite observations for assessing snow and ice resources on Earth have been greatly improved through the utilization of higher resolution imaging systems and multispectral images in the wavelength range from 0.4 μm to 1.55 cm. The possibility that the variation in areal extent of the snow cover may be related by empirical means to the average monthly run-off in a given watershed was demonstrated by comparing run-off records from the Indus River Basin in south-east Asia with a series of snow-cover maps obtained from Nimbus-3 and 4 imagery. Similar studies using the higher spatial resolution available with ERTS-1 imagery were carried out for the Wind River Mountains watersheds in Wyoming, where it was found that the empirical relationship varied with mean elevation of the watershed. In addition, digital image-enhancement techniques are shown to be useful for identifying glacier features thought to be related to extent of snow cover, moraine characteristics, debris coverage, and the like. Finally, longer wavelength observations using sensors on board the Nimbus-5 satellite are shown to be useful for indicating crystal size distributions and onset of melting on glacier snow cover.

RÉSUMÉ. *Satellites—Nouvelles techniques d'observations globales pour la glace et la neige.* Le satellite météorologique TIROS-2 en 1961 avait permis une vue synoptique de zones étendues avec une caméra de télévision à bord. Les possibilités des observations par satellite pour inventorier les ressources terrestres en neiges et glaces ont été fortement augmentées par l'utilisation d'appareils donnant des images à meilleure résolution et des images multispectrales dans les gammes de longueur d'onde de 0,4 μm à 1,55 cm. En comparant les enregistrements hydrologiques du bassin de l'Indus dans l'Asie du Sud-Est avec une série de cartes d'enneigement obtenues avec les images de Nimbus 3 et 4, on a démontré la possibilité de trouver une corrélation empirique entre le débit mensuel moyen d'un bassin versant et la variation de l'étendue de la zone enneigée. Des études semblables utilisant la résolution spatiale supérieure disponible avec les images de ERTS-1 ont été conduites pour les bassins versants des Wind River Mountains dans le Wyoming où l'on a trouvé que la relation empirique variait avec l'altitude moyenne du bassin versant. De plus, en utilisant les techniques de renforcement de l'image par digitalisation, on a montré qu'on pouvait identifier des caractéristiques de glaciers supposés liés à l'étendue de la zone enneigée, les caractéristiques de la moraine, le transport moyen de matériaux et autres données analogues. Enfin, des observations à plus grandes longueurs d'onde utilisant des capteurs à bord du satellite Nimbus-5 ont montré qu'elles pouvaient servir d'indicateur de la distribution des dimensions des cristaux, ainsi que de l'attaque de la fusion sur la couverture neigeuse d'un glacier.

ZUSAMMENFASSUNG. *Satelliten—Neue weltweite Beobachtungsverfahren für Eis und Schnee.* Seit dem Start des TIROS 2-Wettersatelliten im Jahre 1961, der die synoptische Beobachtung weiträumiger Gebiete mit einem Fernsehsystem erlaubte, wurden die Möglichkeiten zur Beobachtung und Abschätzung der Schnee- und Eistrüklagen auf der Erde von Satelliten aus durch die Verwendung von Bildsystemen höherer Auflösung und multispektraler Bilder im Spektralbereich von 0,4 μm bis 1,55 cm wesentlich verbessert. Durch den Vergleich von Abflussdaten für das Einzugsgebiet des Indus in Südost-Asien mit einer Serie von Schneebedeckungskarten aus Nimbus-3 und 4-Bildern wurde gezeigt, dass die flächenhafte Änderung der Schneedecke empirisch zum mittleren monatlichen Abfluss eines bestimmten Einzugsgebietes in Beziehung gesetzt werden kann. Ähnliche Studien wurden unter Ausnutzung der höheren räumlichen Auflösung von ERTS-1-Bildern für die Einzugsgebiete der Wind River Mountains in Wyoming durchgeführt; dabei ergab sich, dass die empirische Beziehung von der mittleren Höhe des Einzugsgebietes abhängig war. Weiter wird gezeigt, dass digitale Verfahren zur Bildverstärkung die Identifizierung von glazialen Erscheinungen erleichtern können, bei denen ein Zusammenhang mit dem Ausmass der Schneedecke angenommen wird, wie Merkmale von Moränen, Schuttbedeckung und ähnliches. Schliesslich wird ausgeführt, dass Beobachtungen mit längeren Wellenlängen durch Sensoren an Bord des Nimbus-5-Satelliten zur Feststellung der Verteilung von Kristallgrössen und des Einsetzens der Schmelze in einer Gletscherschneedecke geeignet sind.

I. INTRODUCTION

The power of observing significant snow and ice features with satellites was first demonstrated when television cameras with relatively modest spatial resolution, mounted on the TIROS-2 weather satellite, monitored the breakup in the Gulf of St. Lawrence during Spring 1961. In that case, only one of several advantages of remote sensing from satellites was brought to bear on the problem of monitoring sea ice; namely, the ability to obtain almost

instantaneously a synoptic view over large areas. Figure 1 demonstrates this capability showing a mosaic made from the Nimbus 3 image dissector camera system (IDCS) on 15 April 1969. Large areas of north-eastern Canada, Baffin Island, Greenland, and Iceland can be seen quite clearly.

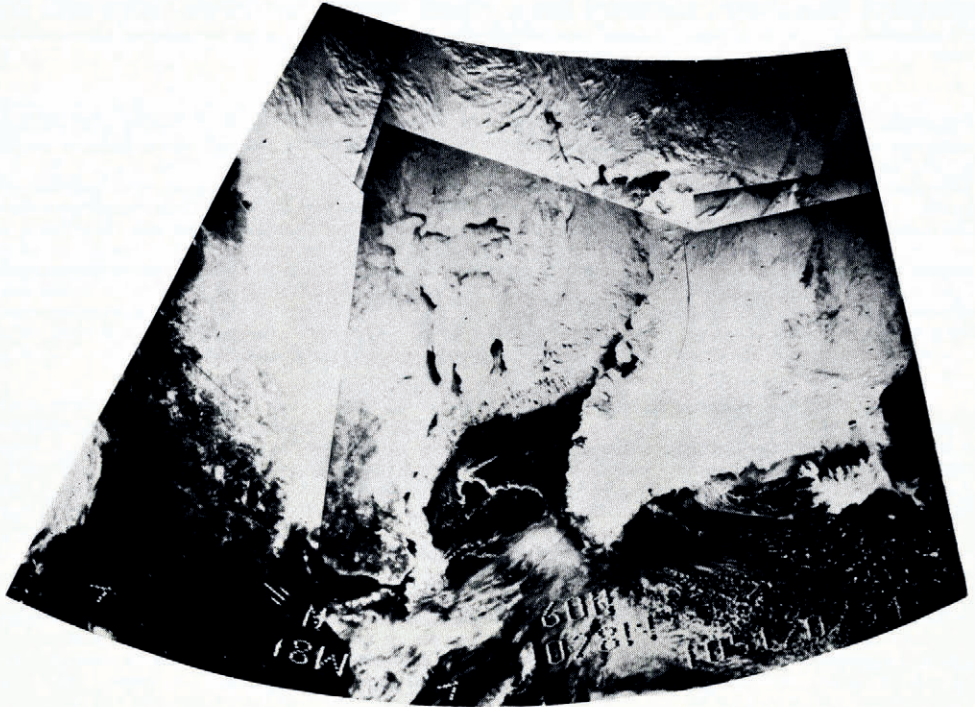


Fig. 1. Satellite photograph of snow and ice conditions in Iceland, Greenland, east Canada, and New England, 15 April 1969.

Observations in many other spectral regions have been made since the visible wavelength TIROS-2 observations were made. These observations in other spectral regions have made it possible to monitor repetitively over extensive areas many important properties of snow and ice that are and have been applied in a useful fashion to many practical situations including navigation and water resources monitoring. In 1964, for instance, Nimbus-1 obtained the first images of infrared emission in the $3.8 \mu\text{m}$ region over Antarctica. Because of the strong contrast in temperature between ice and open water, breaks in the sea ice could be monitored in night-time conditions that occur continuously over polar areas during the winter months.

Observations from the Nimbus-3 high resolution infrared radiometer in the $0.7\text{--}1.3 \mu\text{m}$ spectral region illustrated the utility of these data for delineating regions where active melting was occurring on ice and snow and thus decreasing the reflectance in this spectral region. Figure 2 taken from Nimbus-3 graphically illustrates this in simultaneous views over the southern Sierra Nevada Mountains region in California.

The long life (1–3 years) of Nimbus and NOAA satellites of the late 1960's and early 1970's has permitted reliable, repetitive snow-cover observations of utility for snow-pack monitoring and subsequent run-off prediction. Barnes and Bowley (1968) and McClain and Baker (1969) have described techniques for analyzing and presenting snow-cover observations from meteorological satellites. Figure 3 shows repetitive observations taken by the Nimbus 3

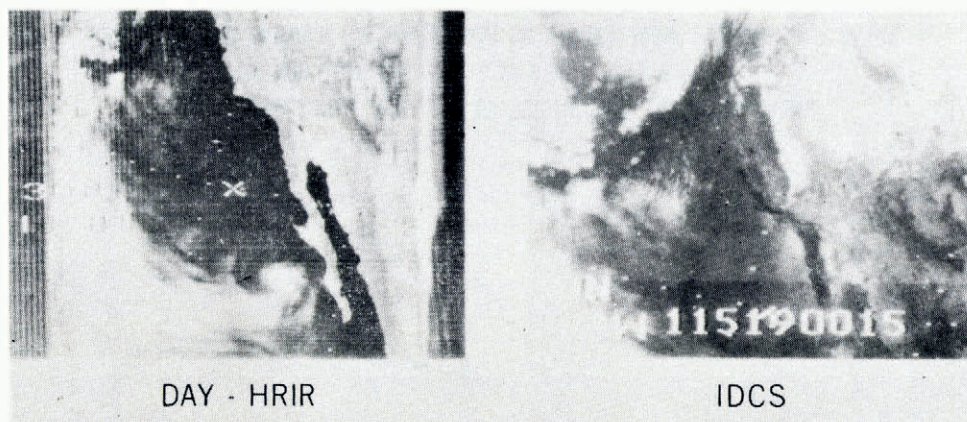


Fig. 2. Simultaneous views of the southern Sierra Nevada Mountains in California obtained in the visible (LDCS) and near-infrared (HRIR) spectral regions.

and 4 IDCS over the Indus River basin in the Himalayan region of south-west Asia. Salomonson and MacLeod (1972) (Fig. 4) showed evidence that these observations may have a usable empirical relationship to observed run-off that could be used for seasonal or monthly run-off prediction in areas lacking conventional information. The IDCS has also been used to provide maps of the polar regions on occasions when cloud obscuration was not a problem. An

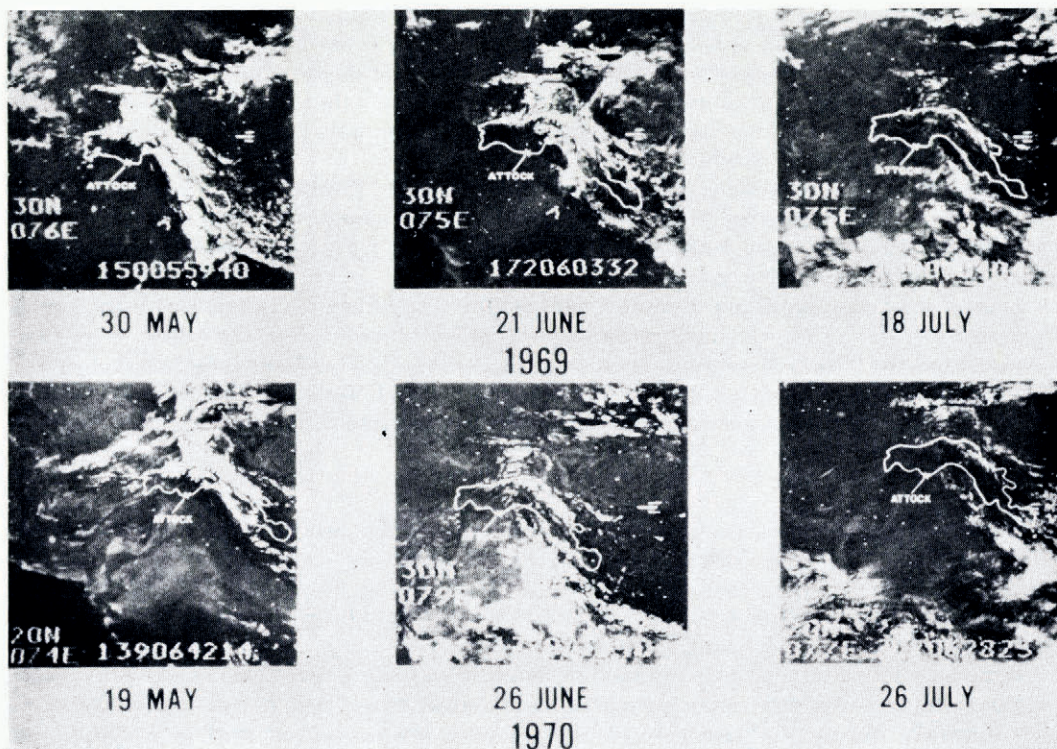


Fig. 3. Nimbus-3 and Nimbus-4 IDCS observations of snow cover over the Indus River watershed during the major snow-melt period.

**AREAL EXTENT OF SNOW COVER AS OBSERVED BY NIMBUS 3 AND 4 IDCS
OVER THE INDUS RIVER WATERSHED VERSUS
MEAN MONTHLY DISCHARGE AT ATTOCK, WEST PAKISTAN**

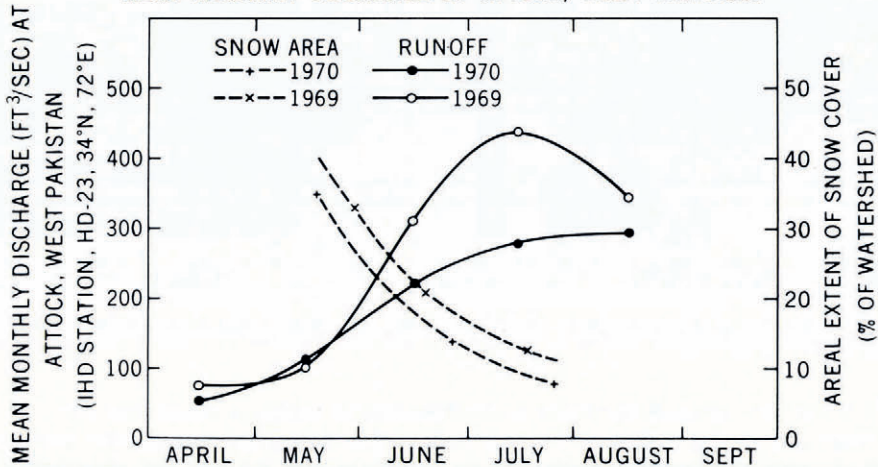


Fig. 4. Aerial extent of snow cover over the Indus River watershed as obtained by the analysis of the images in Figure 3. $500 \text{ ft}^3/\text{s} = 14.2 \text{ m}^3/\text{s}$.

example of such imagery is shown in Figure 5 in which the continent of Antarctica was observed during a series of satellite overpasses on relatively cloud-free days. The outline of the continent is fairly clearly seen. However, the signature of the continent itself is quite uniform except for scattered cloud formations and a few mountain ridges. Unlike the images obtained in snow-covered areas outside the polar regions, there is no bare ground or forestation to provide distinguishable details.

In summary, the early meteorological satellites, TIROS, Nimbus, and ITOS or NOAA provide, or have provided, results of interest and utility for monitoring snow and ice features synoptically over large areas in the visible, near infrared ($0.7\text{--}1.3 \mu\text{m}$), and far infrared (3.8 and $10\text{--}12 \mu\text{m}$) with modest spatial resolution (in general, $>4 \text{ km}$). In the last two years, however, at least two significant breakthroughs in global snow and ice monitoring were made. These involve the relatively high resolution (80 m) observations in the visible and near infrared from the Earth Resources Technology Satellite, ERTS-1, and observations in the microwave portion of the electromagnetic spectrum obtained from the Nimbus-5 spacecraft. The following sections describe representative and relevant results from these two spacecraft.

II. ERTS-1 RESULTS

ERTS-1 was launched on 23 July 1962 into a near polar, sun-synchronous orbit at an altitude near 900 km . The orbital characteristics are nominally such that the multi-spectral scanner subsystem (MSS) on ERTS-1 is capable of taking observations of cartographic quality in the $0.5\text{--}0.6$, $0.6\text{--}0.7$, $0.7\text{--}0.8$ and $0.8\text{--}1.1 \mu\text{m}$ spectral regions over any given point on Earth once every 18 d, cloud cover and sunlight permitting. The convergence of the orbits at high latitudes makes it possible to monitor individual ice floes, cracks and leads, polynyas, and icebergs more often than 18 d and in some areas features can be monitored on daily intervals. Results from analysis of ERTS-1 data involving snow and ice mapping are provided in Freden and others (1973) and a review is provided by Salomonson and Greaves (1974).

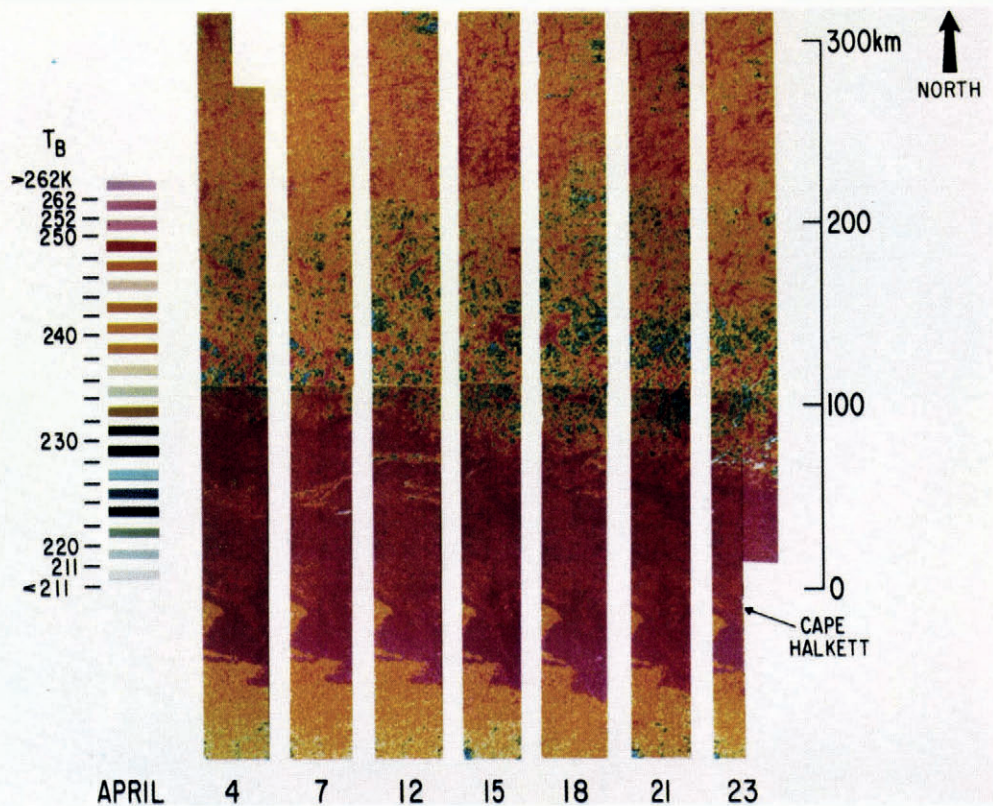


Fig. 7. Time sequence of microwave ($\lambda = 1.55$ cm) mosaic maps of sea ice in the southern Beaufort Sea. The maps extend from Cape Halkett on the western side of Harrison Bay north for approximately 350 km.

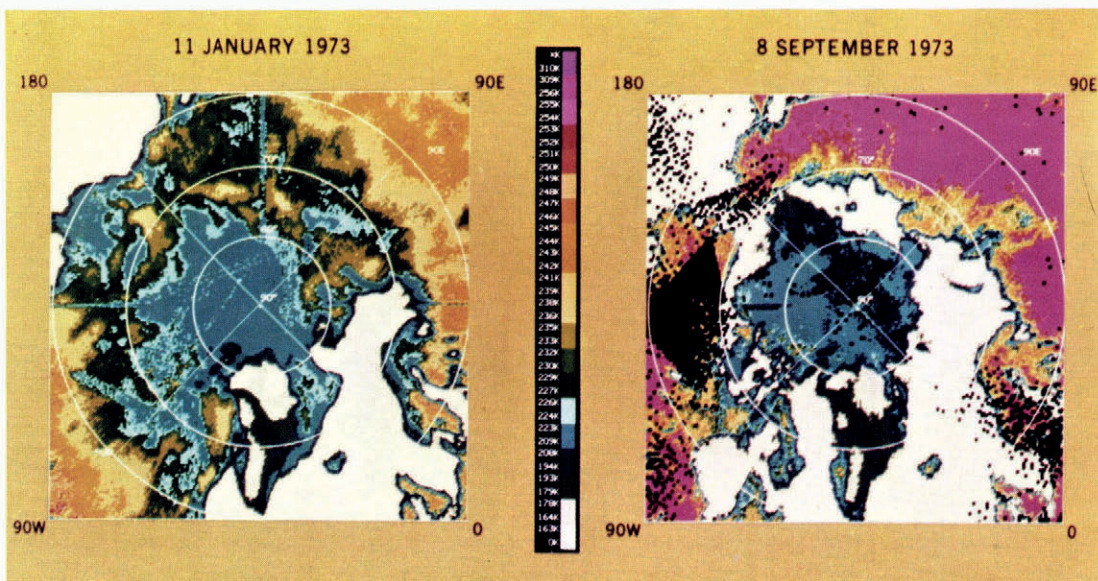


Fig. 9. Seasonal changes in the extent of the Arctic ice pack as shown in the ESMR imagery (false color).

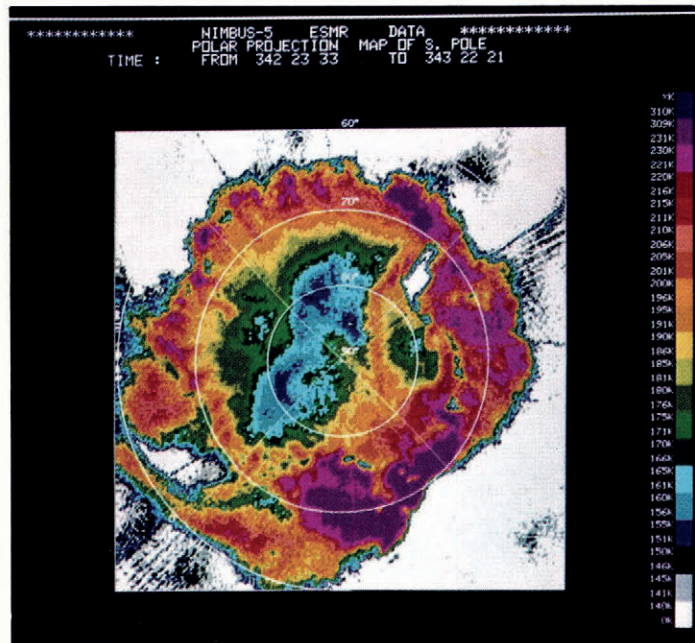
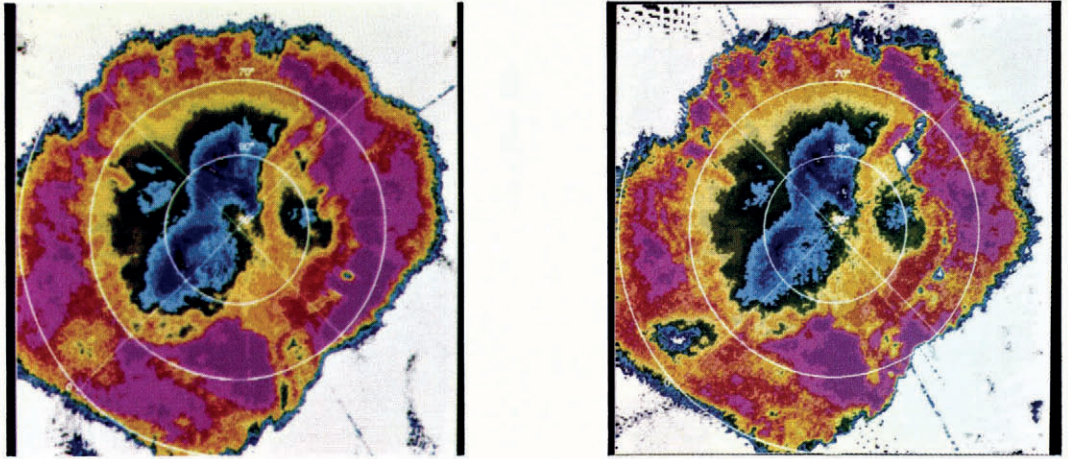


Fig. 11. Three sequential ESMR images of the Antarctic showing the rapid development of major polynyas and leads: A. 18 November 1973, B. 27 November 1973, and C. 9 December 1973.

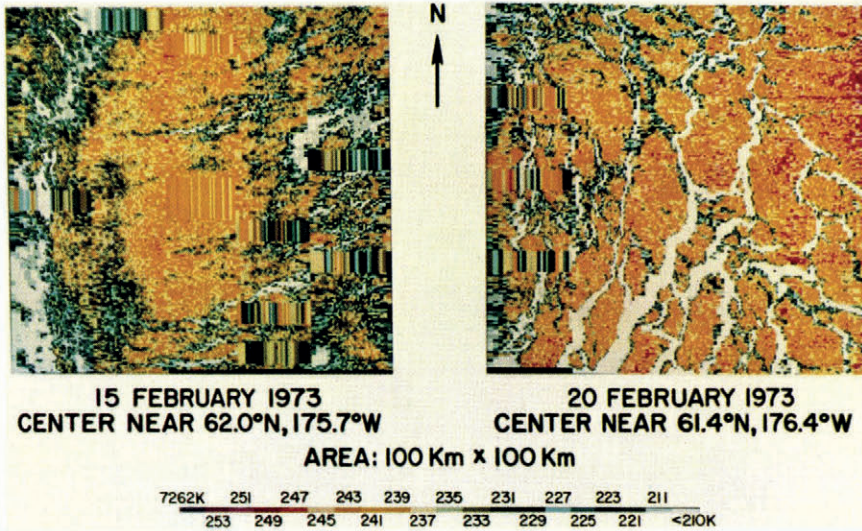


Fig. 12. False-color representations of the passive microwave imagery (1.55 cm) from the sea-ice test areas studied by the U.S. team during BESEX. The mosaics were assembled in a computer from the individual data points obtained during the five-track aircraft flight pattern. The regions of elongated color strips represent periods of instrumentation malfunction (Gloersen and others, 1974[b]).

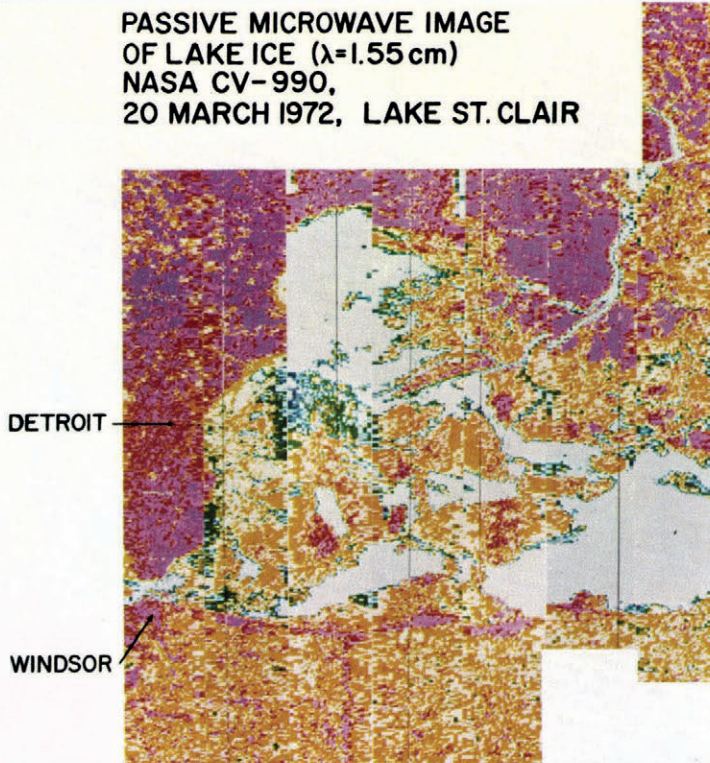


Fig. 13. Passive microwave image ($\lambda = 1.55\text{ cm}$) of lake ice in Lake St. Clair on 20 March 1972. The brightness temperature corresponding to the uniform grey tone indicates open water. Where the colors show light and dark blues (cold) the ice is thinner than where the colors indicate red, violet, and orange (warmer).

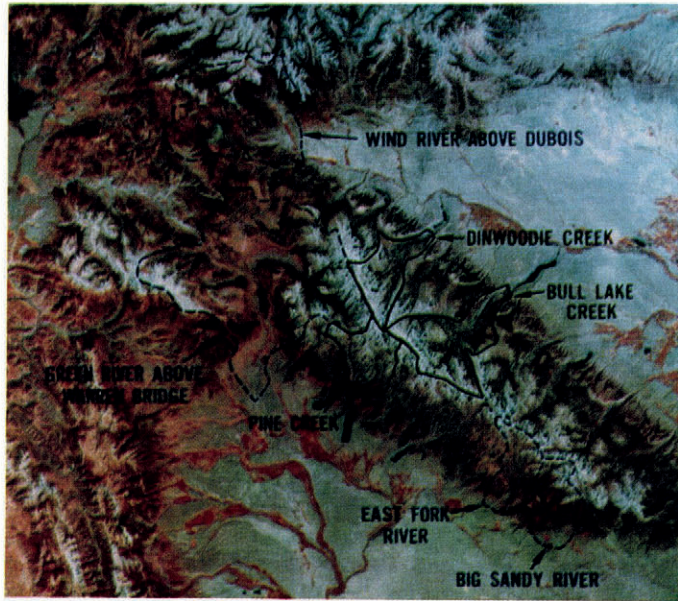


Fig. 6. False-color composite view of Wind River Mountains of Wyoming obtained from the ERTS-1 satellite, 6 August 1972. Watershed boundaries are indicated, those in blue <math>< 10\,000\text{ ft}</math> ($3\,050\text{ m}$), those in black >math>> 10\,000\text{ ft}</math> (>math>3\,050\text{ m}</math>) mean elevation.

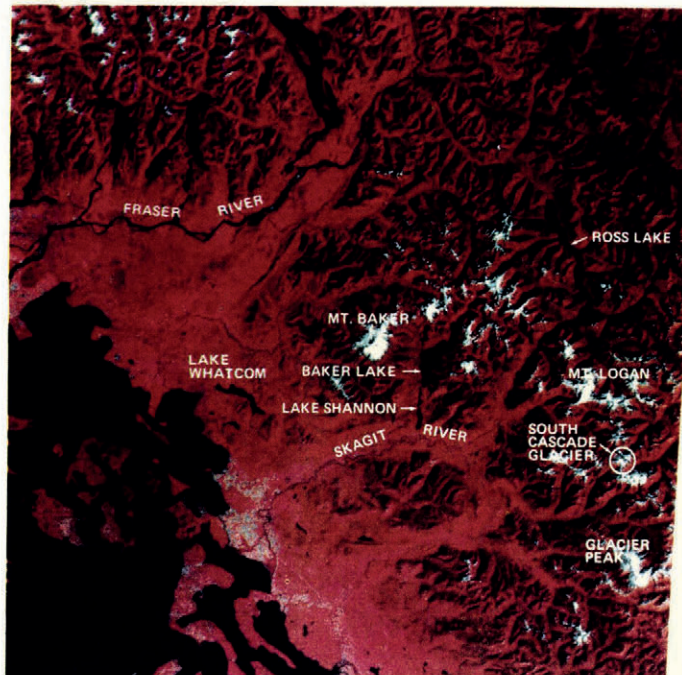
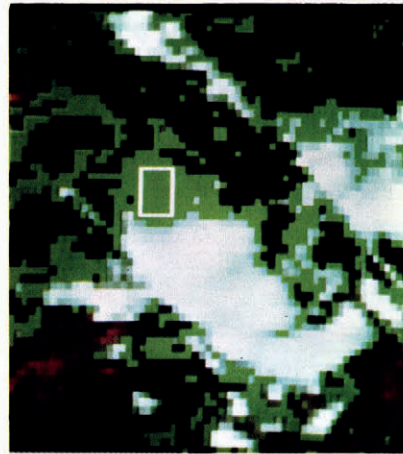
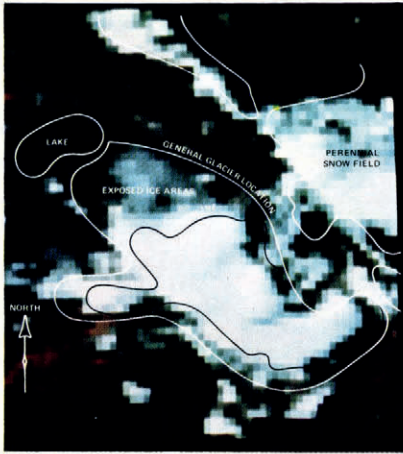
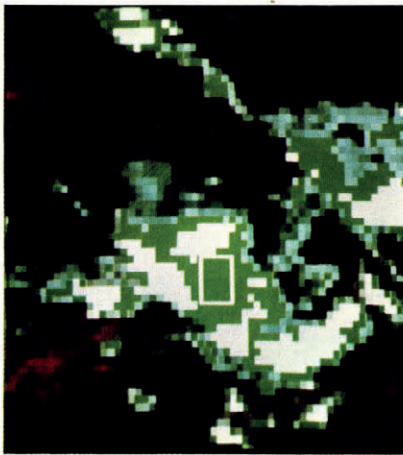


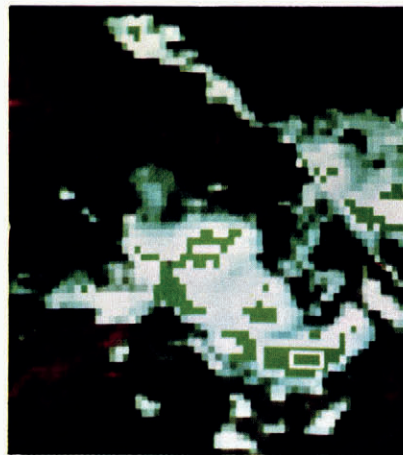
Fig. 8. An ERTS-1 $185\text{ km} \times 185\text{ km}$ image reproduced from observations acquired on 16 September 1973 over Washington State. South Cascade Glacier appears at the lower right.



(a)



(b)



(c)

Fig. 9. Expanded views of South Cascade Glacier. Digital data from the 0.5–0.6 μm , 0.6–0.7 μm , and 0.8–1.1 μm imagery was displayed on a television screen and photographed and parallelepiped classifications performed.

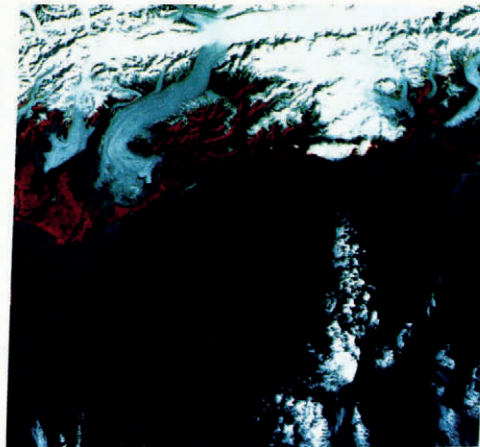


Fig. 10(a)
22 September 1972.

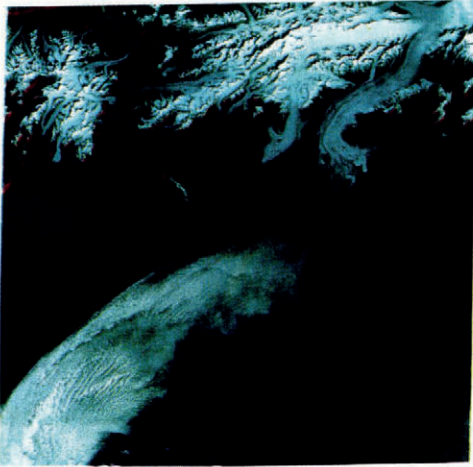


Fig. 10(b)
18 September 1973.

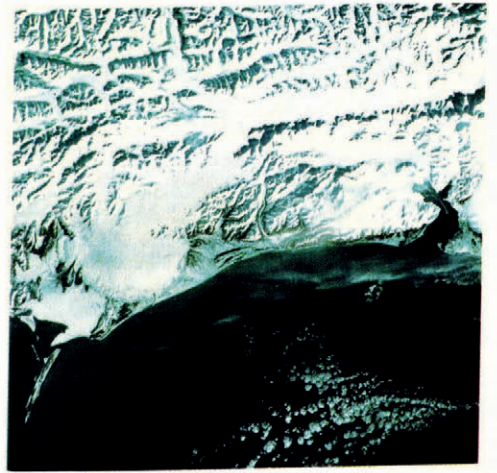


Fig. 10(c)
26 February 1974.

Fig. 10. Three ERTS-1 185 km × 185 km images over the Bering Glacier in south-central Alaska.

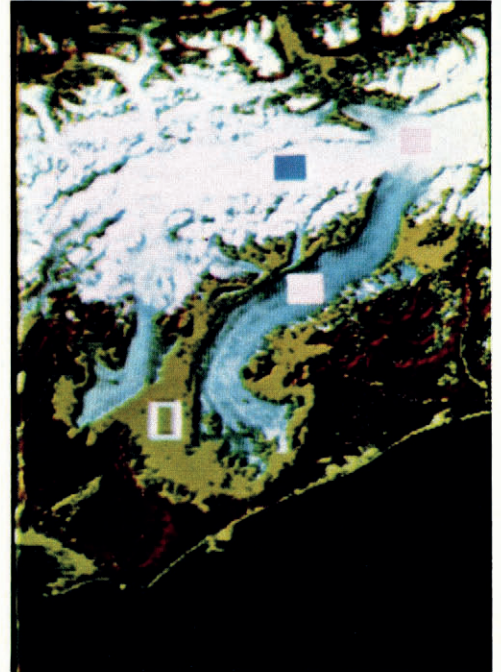
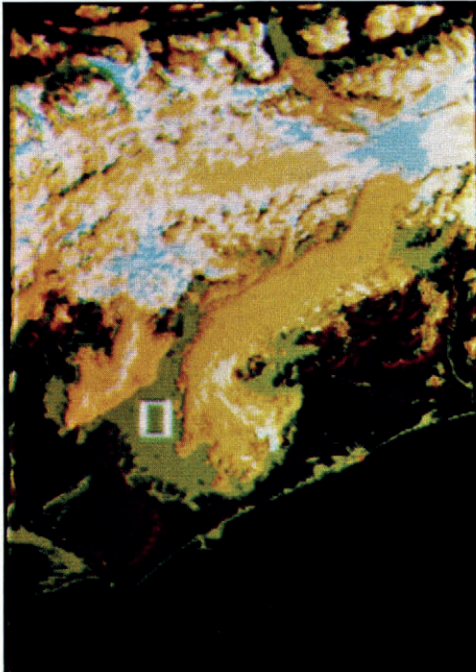


Fig. 11. Two views of the Bering Glacier showing a partially classified scene (left) and the selected areas used to classify more completely the same scene (right) (ERTS-1 22 September 1973).

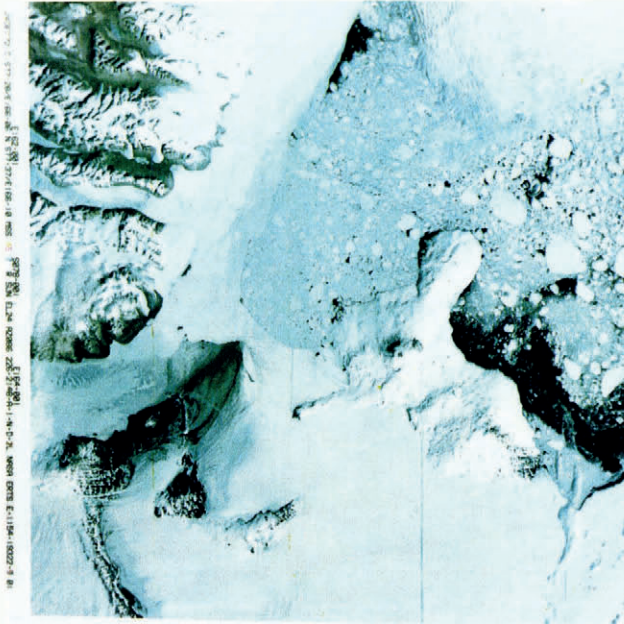


Fig. 13. Image of the Ross Ice Shelf region in Antarctica obtained from the ERTS-1 satellite.

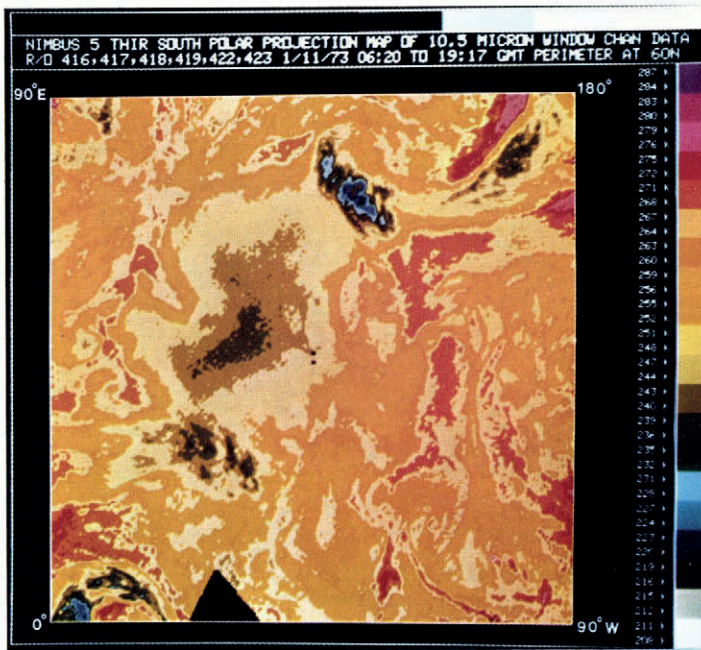


Fig. 14. Image of Antarctica obtained from the Nimbus-5 THIR on 11 January 1973.

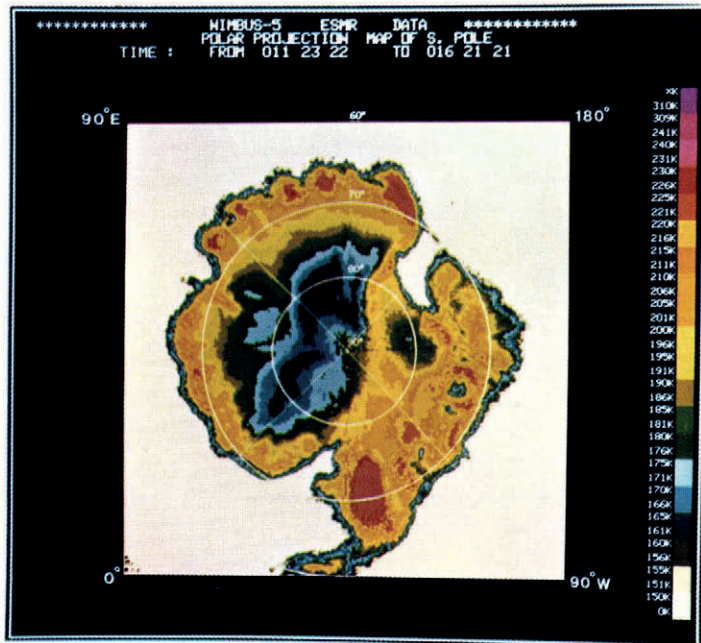


Fig. 15. Image of Antarctica obtained from the Nimbus-5 ESMR, averaged over five days starting on 11 January 1973.

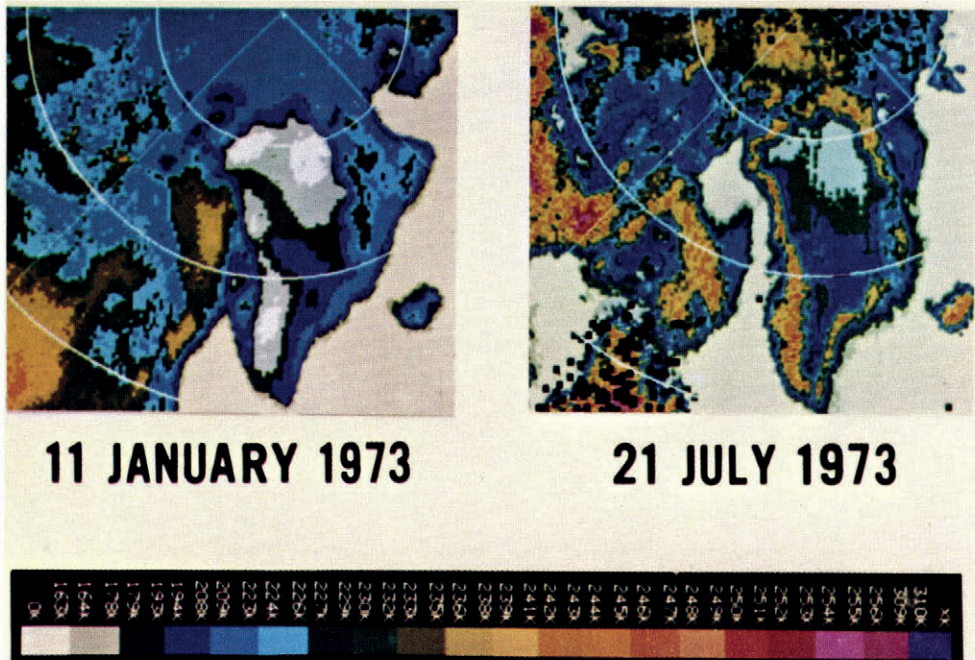


Fig. 19. The image of Greenland obtained from 1.55 cm microwave data for the summer and winter seasons (11–16 January 1973 and 21 July 1973).

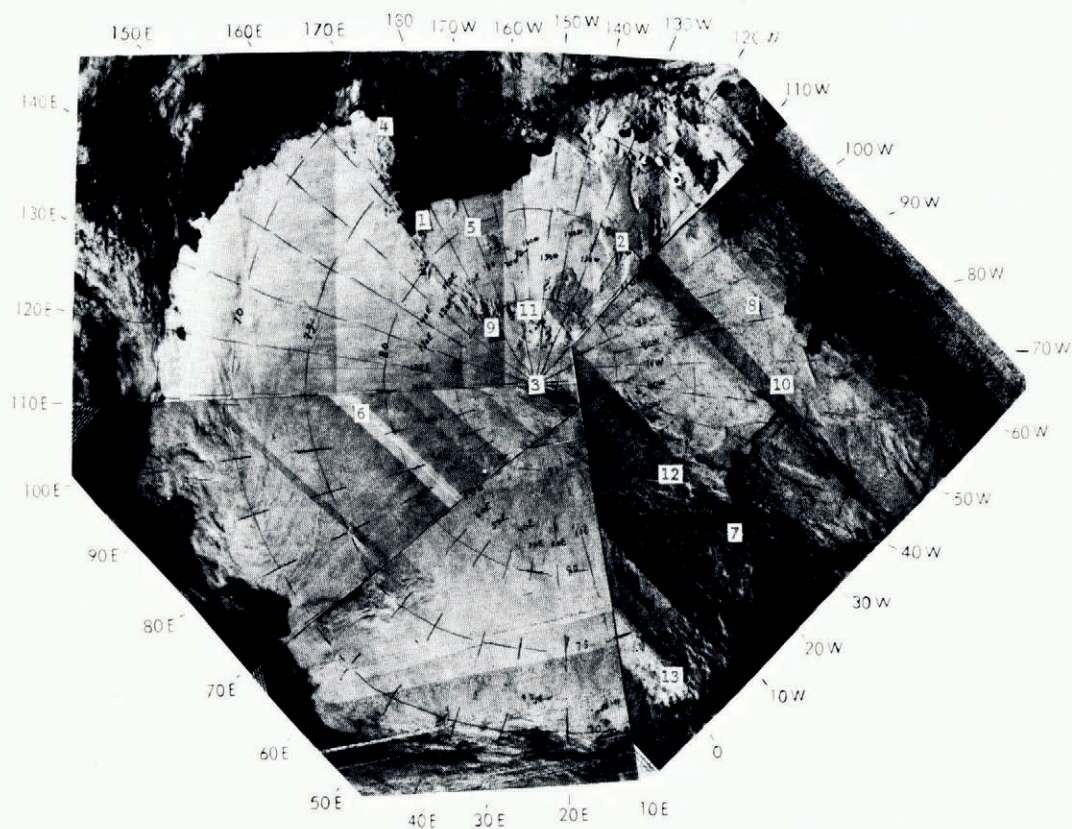


Fig. 5. *Nimbus-4* IDGS observation of Antarctica. Marked stations and camps are as follows: 1: McMurdo (U.S.A.) and Scott Base (New Zealand). 2: "Byrd" (U.S.A.). 3: South Pole (U.S.A.). 4: "Hallett" (U.S.A.). 5: "Brockton" (U.S.A.). 6: "Vostok" (U.S.S.R.). 7: Halley Bay (U.K.). 8: "Siple" (U.S.A.). 9: "McGregor" (U.S.A.). 10: "Lassiter" (U.S.A.). 11: "Amundsen" (U.S.A.). 12: "Shackleton" (U.K.). 13: Dronning Maud (Norway).

In terms of snow-pack monitoring, activities at Goddard Space Flight Center have centered on the use of ERTS-1 data in the Wind River Mountains of Wyoming. The principal objective has been to see if snow-cover area observations may be useful in empirical fashion to better characterize and perhaps predict run-off from watersheds in these mountains. Figure 6 (pl. IV) shows how the Wind River Mountain area appears from ERTS-1. Watershed boundaries for seven watersheds in which snow-mapping from ERTS has been accomplished are delineated on this figure. Three of the watersheds have mean elevations above 3 km and four of the watersheds have mean elevations below 3 km.

During the 1973 snow-melt season several cloud-free views of the watersheds mentioned above were obtained. The percentage of each basin covered by snow was plotted versus time along with the variation in the 18 d mean flow per unit area for each of these watersheds. In order to see if it is possible to demonstrate that major physiographic differences affect the character of snow-cover depletion curves, the results for the three high watersheds and the four low watersheds were compiled and average results obtained. The normalizing factors used in comparing the results consisted in using specific run-off (per unit area) rather than the total volume of run-off. The results of this procedure are shown in Figure 7. The principal point

to be made concerning this figure is that the general character of the specific run-off and snow-cover variation between high and low watersheds (mean elevation >3 km and <3 km respectively) can be seen to be distinctly different. The specific run-off from the lower watersheds has a smaller peak flow that occurs earlier in time. These characteristics are consistent with the snow-cover depletion curve which shows the snow cover disappearing more rapidly with time due to smaller snow depths and the higher temperatures at the lower altitudes. Of course, several years of data are necessary in order to establish rigorously the utility of this kind of approach for a given watershed. Along these lines, analyses of the 1974 ERTS-1 snow-cover observation are continuing.

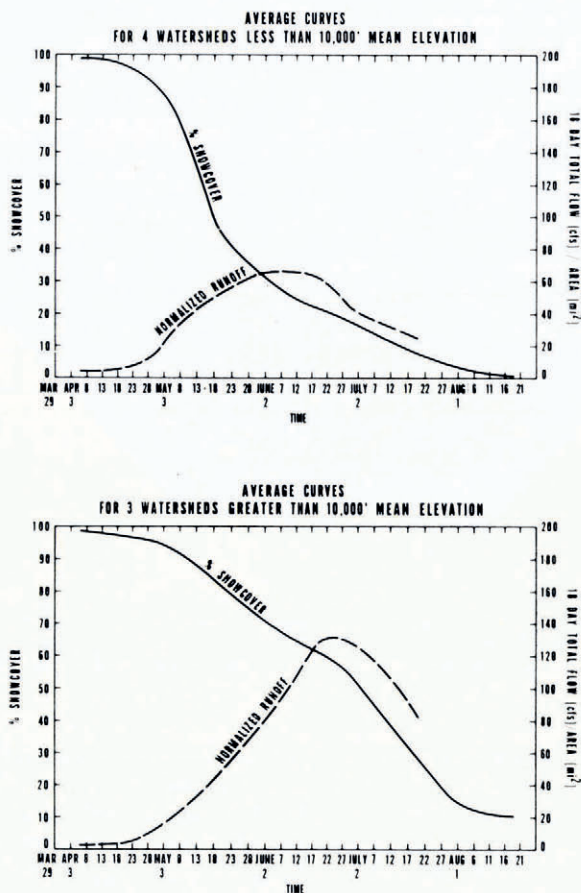


Fig. 7. Average snow-cover depletion and run-off for the Wind River Mountain watersheds during 1973 as obtained by analyzing ERTS images such as those shown in Figure 6. $200 \text{ ft}^3/\text{s mi}^2 = 1.09 \text{ m}^3/\text{s km}^2$.

The ERTS-1 data have been found to be particularly exciting for the monitoring and study of glaciers and their attendant surface features. The character of medial and terminal moraines, the extent of snow cover, debris, and other features can be observed repeatedly and related to the mass balance of the glacier and its movement. Of particular interest has been the use of these observations to locate or monitor surging glaciers. The Yentna Glacier near Mt McKinley, Alaska, and the Tweedsmuir Glacier in British Columbia, Canada, are among those glaciers of this type whose recent surges have been monitored from ERTS-1.

Not a great deal of analysis has been accomplished and reported in the recent literature in which ERTS-1 digital data and objective feature classification have been employed in glaciological studies. The utilization of digital data commonly allows one to extract more detail and analytical numerical information than one can obtain simply from photographic enlargement and processing. To illustrate these points, ERTS scenes taken over the Bering Glacier (lat. 60° N., long. 144° W.) in south-central Alaska and the South Cascade Glacier (lat. $48^{\circ} 30'$ N., long. 121° W.) in Washington state were examined using ERTS digital data stored on computer compatible tapes. Figure 8 (pl. VI) shows the entire $185 \text{ km} \times 185 \text{ km}$ color composite image taken over Washington State on 16 September 1973. The location of the South Cascade Glacier is outlined by a small circle covering an area that is approximately 6.5 km in diameter.

Figure 9 (pl. V) shows this same area expanded many times so that more detail can be seen than is discernible on the previous figure. Sketch lines have been superimposed to show the areal extent of major features in this expanded view of the glacier. Portions a, b, and c of Figure 9 show what portions of the glacier appear to have the same multispectral character as each of the small areas enclosed in the white rectangles. By this, we mean that the digital reflectance values obtained for the 0.5–0.6, 0.6–0.7, and 0.8–1.1 μm band MSS observations agree within a pre-specified tolerance. In Figure 9a, b, and c, all areas that appeared the same as the selected areas are displayed as a green color. Using such data-processing equipment* one can select a known area and in a few seconds classify the remainder of the scene to see how many other areas are similar in a multi-spectral sense. Also, one can measure areas or obtain other statistical information that may be appropriate. As another example, Figure 10 (pl. V–VI) shows three $185 \text{ km} \times 185 \text{ km}$ color composite views of the Bering Glacier reflecting seasonal and annual changes. Figure 11 (pl. VI) shows a partially classified September 1972 scene depicting selected areas in various colored squares and a more completely classified scene employing each of the selected samples. The classifications represent the more debris-laden, exposed ice portions of the glacier (area marked by white, open square), the cleaner, less debris-covered, exposed ice portions of the glacier (white solid square) and the snow-covered regions of the snow fields feeding the glacier (blue, solid square). These classifications or variations thereof can be accomplished in only a few minutes and quantitative supporting data provided shortly thereafter such as the number of data elements, or the area comprising each classification.

III. NIMBUS-5 RESULTS

Nimbus-5 was launched on 11 December 1972 into a near polar sun-synchronous circular orbit at an altitude of about 1100 km. In addition to the infrared and microwave atmospheric sounders on board, the spacecraft contains three imaging devices in the infrared and microwave regions. The highest spatial resolution is achieved by the surface composition mapping radiometer (SCMR) which has three spectral intervals from 8.3–9.3 μm , 10.2–11.2 μm and 0.8–1.1 μm . The instantaneous field of view of this instrument is 0.6 mrad providing a nadir ground resolution cell size of about 660 m. An example of the imaging quality available from this device is shown in Figure 12 which depicts the Ross Ice Shelf in Antarctica. The structural detail shown in this image is excellent, but the technique suffers for significant fractions of the observing time from obscuration by cloud cover. Features evident in this figure include open water in the Ross Sea, bare terrain in the McMurdo area, and scattered clouds. As in the IDCS image (Fig. 5), the structural details on the continental ice sheet are lacking. Increasing the spatial resolution apparently does not help in bringing out the details in the ice sheet as is

* The data-processing equipment used here is commercially known as the General Electric Image 100 and is located at the General Electric offices in Beltsville, Maryland. Particular appreciation is expressed to William Dallam who greatly facilitated the generation of the material referred to above.

shown from the ERTS image of the McMurdo area in the Ross Sea (Fig. 13, pl. VII). While the open water, bare terrain, and bare glaciers are clearly depicted, it is evident that as the higher elevations are reached the details become less and less pronounced.

The temperature-humidity infrared radiometer (THIR) is a two-channel scanning radiometer with considerably lower spatial resolution. One channel ranges from 6.5–7 μm , with a 21 mrad field of view, and the other from 10.5–12.5 μm with a 7 mrad field of view. The latter channel is used for observing the surface in the absence of clouds. THIR provides

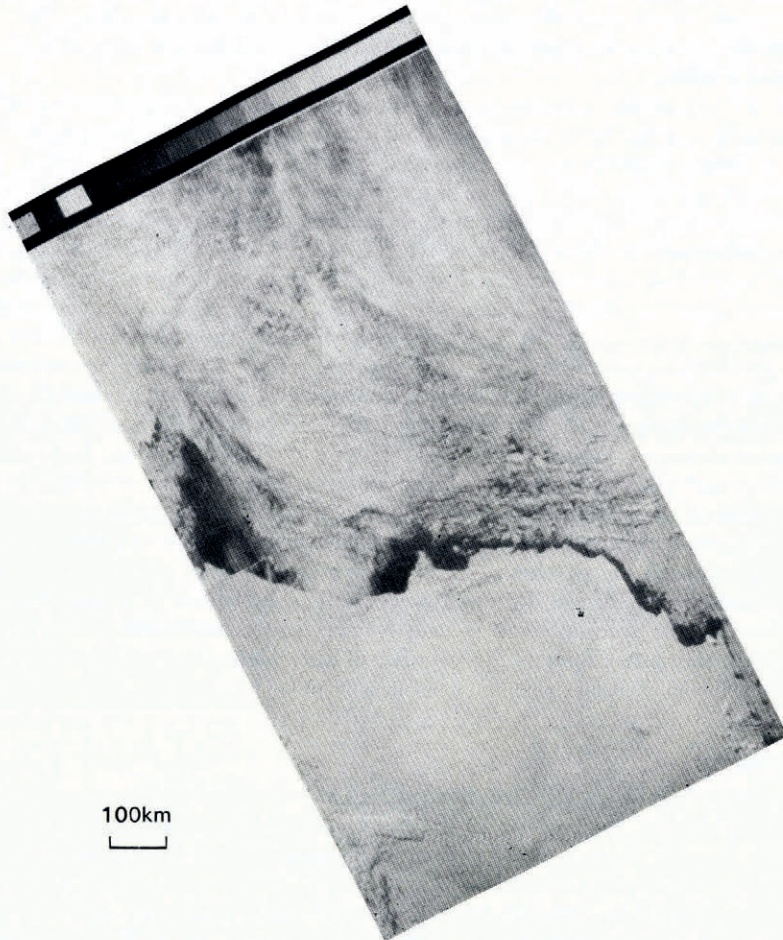


Fig. 12. Image of a portion of the Ross Ice Shelf region in Antarctica obtained from the Nimbus-5 SCMR. Ross Island is near the center of the left-hand edge of the image. The other extremity of the ice shelf edge is about $\frac{2}{3}$ of the image width from the left-hand edge.

valuable information on surface temperature when atmospheric conditions permit. In Figure 14 (pl. VII), there is shown a polar stereographic projection of THIR data from the 10.5–12.5 μm channel of the South Polar region. In this image, the continent of Antarctica was largely cloud-free except in the region of the Ross Ice Shelf where a cloud system intruded over the continent from the South Pacific Ocean. Generally speaking, however, the edge of the floating ice pack is obscured by persistent cloud cover in this image. Also, the continental outline is not clearly depicted.

The electronically scanned microwave radiometer (ESMR) on board the Nimbus 5 provides daily coverage over both the polar regions. The ESMR receives radiation emanating from the Earth at a wavelength of 1.55 cm. In this wavelength region and over the temperatures encountered, the Rayleigh–Jeans approximation to the radiation law applies. That is, the radiative power received is proportional to the first power of the brightness temperature of the radiator which, in turn, is a product of the physical temperature of the radiator and its emissivity. Thus the images produced by the ESMR contain information both on the temperature variation over the surface of the Earth and the variation of the emissivity for different Earth surfaces. Radiation received at 1.55 cm originates both from the atmosphere of the Earth and its surface. In particular, the atmospheric contributions come both from water vapor (the wing of the 22.2 GHz water-vapor line) and from liquid water in clouds. Only under conditions of extensive heavy rainfall does the entire contribution come from the atmosphere. The applications of the ESMR imagery in terms of meteorological phenomena over the oceans have been described by Wilheit and others (1973). The atmospheric contribution is the greatest in the tropical regions. In the Arctic and Antarctic, the liquid water and water-vapor contributions become negligible so that the surface can be observed all the time.

The utility of the ESMR in observing sea ice and continental sheet ice has been described previously (Gloersen and others, 1973[a], [b]; Campbell and others, 1974). Dr Campbell will discuss in some detail in another paper at this symposium (Campbell and others, 1975) the sea-ice data obtained in the Arctic and Antarctic regions from the ESMR. For the purposes of illustrating the utility of this technique, Figure 15 (pl. VIII) shows an image of the

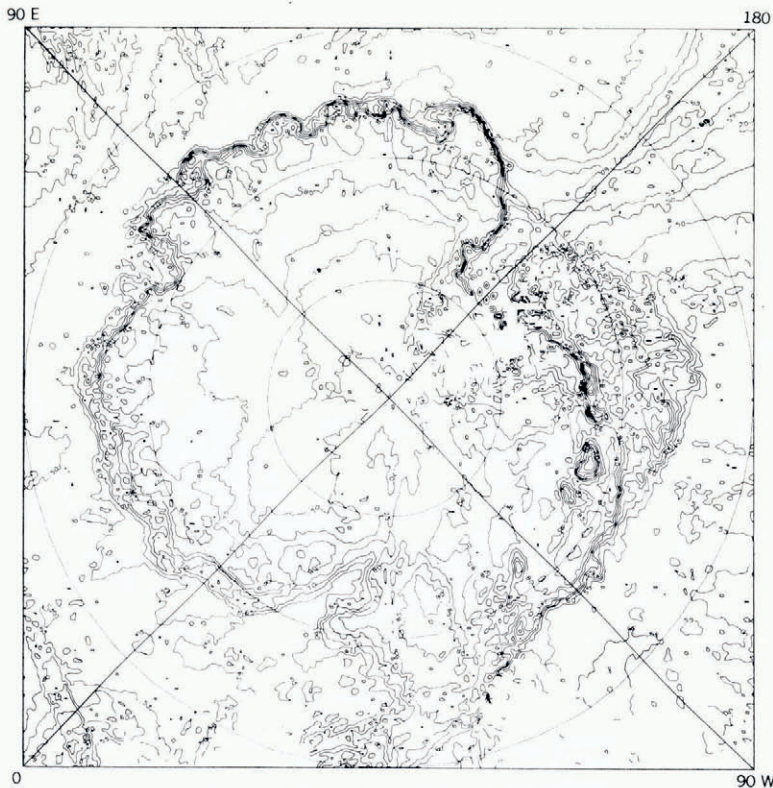


Fig. 16. Isoemissivity contours for a wavelength of 1.55 cm on the Antarctic continent obtained by combining ESMR and THRI data obtained on 11 January 1973 (Figs. 12 and 13).

South Polar region for the same date on which the THIR image was shown in Figure 14. The sea ice surrounding Antarctica appears to have the characteristics of first-year ice, that is, ice with salinity content of 1‰ or more in the freeboard portion of the ice. The emissivity of such ice is 0.95 or greater at a wavelength of 1.55 cm based on aircraft measurements in the Arctic area (Gloersen and others, 1973[a], 1974). The fact that this signature is present in the Weddell Sea is surprising inasmuch as the ice pack in this region persists from one year to the next, according to the ESMR data acquired since November 1972 and the observations of workers in the field (private communication from W. F. Weeks).

Combining the THIR and ESMR images over the continent, one can obtain contour maps illustrating the variation of emissivity of the continental ice sheet (Fig. 16). These contours result from a combination of two factors: (1) the physical temperature on the ice surface is lower at the higher elevations and (2) the crystal size distribution in the ice sheet differs in various geographical locations. It should be pointed out that what has been designated as emissivity is actually the ratio of the brightness temperatures at 1.55 cm and 11 μm . However, from computations based on a Mie scattering model it can be shown that the microwave radiation penetrates this ice sheet to a depth of the order of 10 wavelengths (Chang and Gloersen, unpublished). Therefore, the contours in Figure 16 only approximate the true emissivity since the THIR provides the temperature at the surface and the ESMR the average brightness temperature of about a 15 cm layer. On the basis of the Mie scattering model (Chang and Gloersen, unpublished), the contours in Figure 16 may reflect distributions

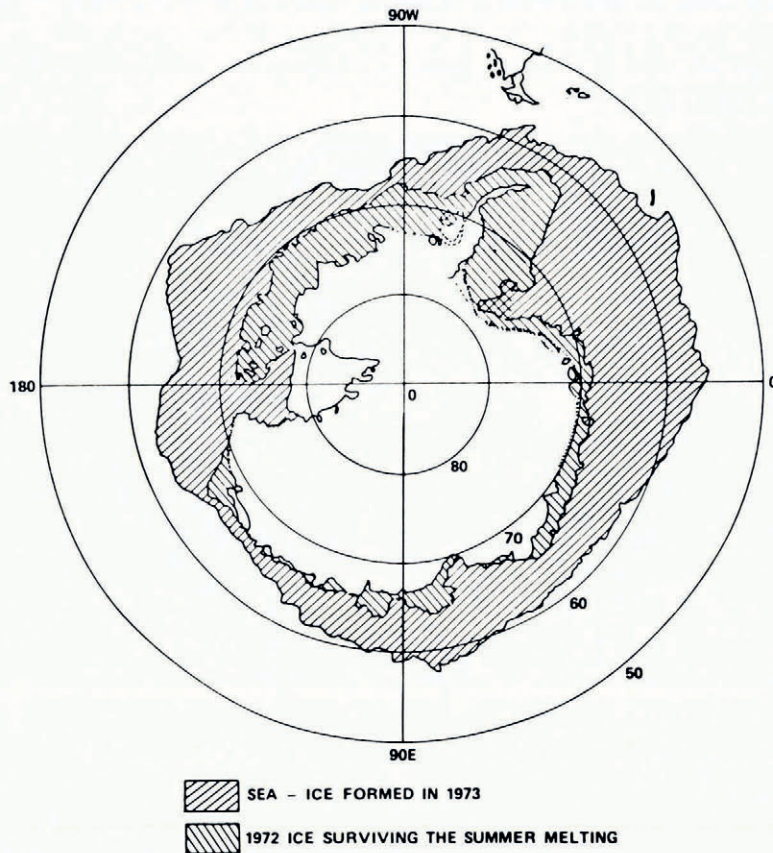


Fig. 17. Near-minimum and near-maximum Antarctic sea-ice boundaries for 1973 (10 February and 16 July).

in the average crystal size on the continent. This model predicts that the lowest emissivities will correspond to the largest average particle sizes, within the range of particles encountered on the continental ice sheet. The size of the particles does depend on the morphology of the ice in a particular region, which has some connection with the temperature range and proximity to open water in that region.

The ESMR images can be used also to observe the variation of the sea-ice coverage with time. The approximate maximum and minimum sea-ice coverage in the South Pole region for 1973 as determined from the ESMR imagery is shown in Figure 17. The variation of ice concentration can also be inferred from these images, even when open water cannot be resolved by the ESMR, by using a linear interpolation between the emissivity of open water (0.4 at a wavelength of 1.55 cm) and that of first-year sea ice (0.95 or greater). The accuracy of this determination is better than ten percentage points; the error is largely due to the uncertainty of the actual temperature of the ice surface within a season. An example of an ice concentration map of Antarctica is shown in Figure 18. The ice concentration parameter is important not only for maritime interests but also for global weather models inasmuch as

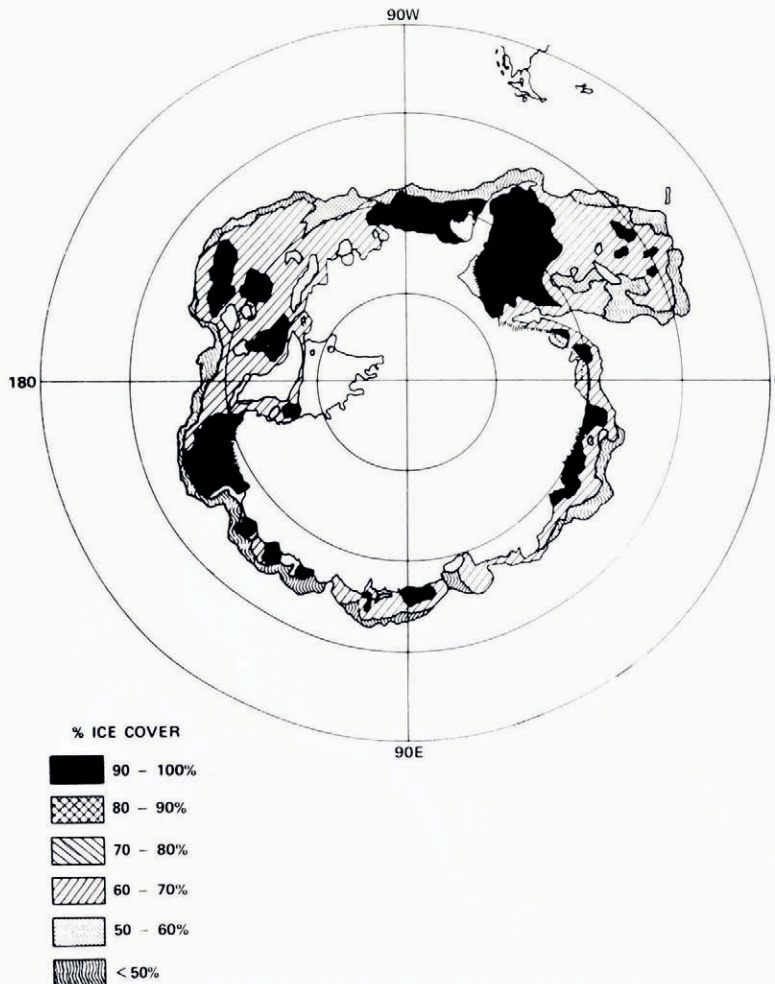


Fig. 18. Compactness of sea ice around Antarctica on 26 December 1972.

the heat transfer rate between the surface of the Earth and the atmosphere is strongly affected by the ice concentration.

The continental ice sheet on Greenland has remarkably different properties from that of Antarctica. In Figure 19 (pl. VIII), two ESMR images of Greenland are shown, one for the summertime and one for mid-winter. One can see a persistent brightness-temperature pattern also in this continental ice sheet. However, it should be noted that the brightness temperatures are the highest at high elevations, quite contrary to what is observed in Antarctica. The emissivity range on Greenland is illustrated in Figure 20, showing a range of emissivities similar to, but a spatial distribution completely different from, those observed in Antarctica. It is not surprising that the crystal size distribution in Greenland, as implied by the variation in emissivity, should be different from that of Antarctica because (1) the range of physical temperatures encountered includes the freezing point of water in Greenland but not at all in Antarctica and (2) inland points in Greenland are considerably closer to open water than in Antarctica. That is to say, the metamorphosis of snow would be expected to be completely different in regions where thawing and freezing occur as opposed to regions where temperatures are always well below freezing.

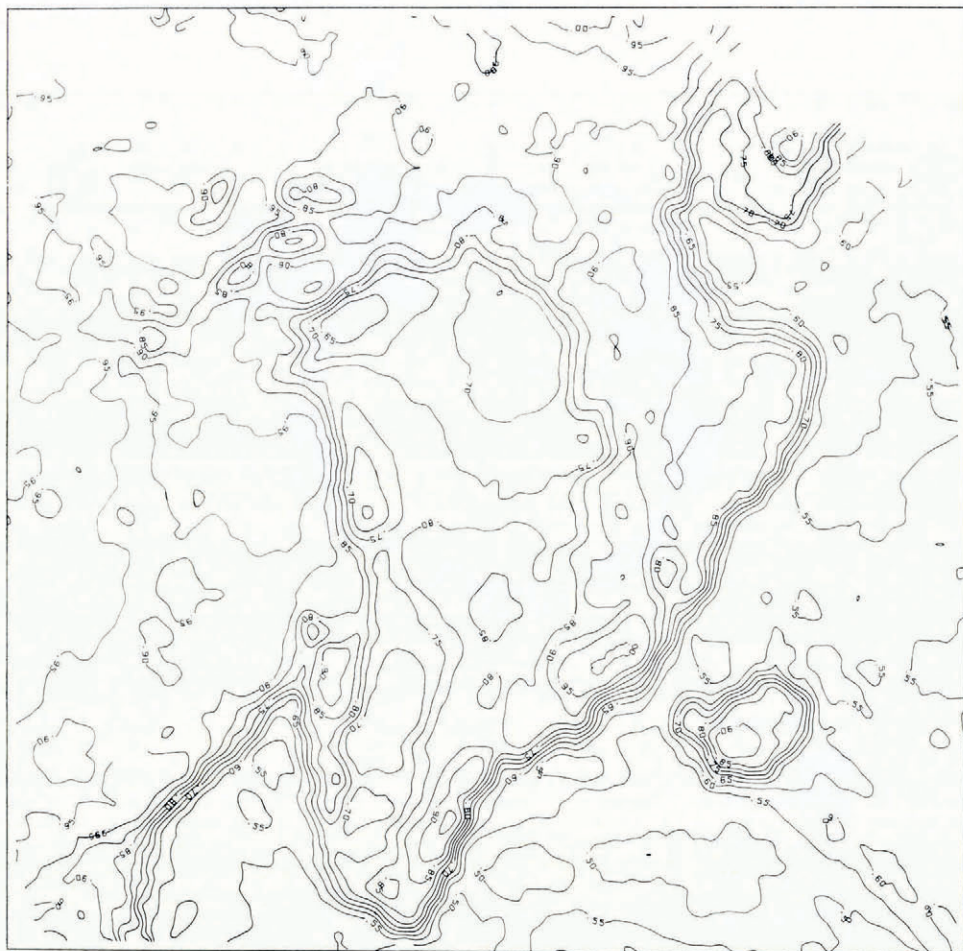


Fig. 20. Isoemissivity contours for a wavelength of 1.55 cm on Greenland obtained by combining ESMR and THIR data obtained on 11 January 1973.

Over the two-year observational period of the Nimbus-5, no significant changes have been observed in the emissivity contours in Greenland or Antarctica. On a long-term basis, changes in these patterns might be observed and could be indicative of slow climatic changes.

Seasonal changes in the continental ice sheet of Greenland, much stronger than those resulting from the seasonal change in physical temperature, have been observed at the lower elevations where thawing and freezing take place. Edgerton and others (1971) have observed that wet snow results in a very much higher microwave brightness temperature than dry snow for snow of sufficient depth. This has been observed also from the ESMR on Nimbus 5 in both the multi-year portions of the Arctic Sea ice canopy and in the lower elevation regions



Fig. 21. The thick solid line is the summer melt line in the snow field covering the Greenland continental ice sheet as deduced from Nimbus 5 ESMR data obtained on 21 July 1973. The area to the east of the thick dashed line is that in which the highest microwave brightness temperatures were observed on 11 January 1973 (cf. Fig. 19).

of Greenland. It is possible that this phenomenon may be utilized to determine any changes in the snow-melt line in Greenland from one year to the next. An attempt has been made to estimate the snow-melt line on the continental ice sheet of Greenland based on the data available at the time of writing. The results are shown in Figure 21. The applicability of this technique must be confined presently to enormous glaciers such as the Greenland ice sheet because of the limited spatial resolution capabilities of the ESMR. However, when higher spatial resolution becomes available in the future, this technique may be extremely valuable in defining snow and firn lines on smaller temperate glaciers.

IV. PROSPECTS FOR THE FUTURE

Continued improvements are envisioned for the future in terms of improved sensors and spacecraft systems with longer lifetimes. In the Earth resources survey area as it relates to snow and ice measurements, it is planned that ERTS-B will be launched in early 1975 or very shortly after ERTS-1 becomes inoperative. ERTS-B will have the same spectral observation and spatial resolution capability as ERTS-1. An ERTS-C is planned for the 1977 time frame with an additional 10–11 μm thermal infrared observation capability.

As has been indicated in the preceding section, the microwave portion of the electromagnetic spectrum holds considerable potential for snow and ice mapping. In the immediate future another ESMR, this one operated at a wavelength of 0.8 cm and with both polarization components, is scheduled for launch on board Nimbus-F late in 1974. The next improvements in spacecraft instrumentation will be flown on the Nimbus-G in the form of a scanning multi-channel microwave radiometer (SMMR). Measurements will be acquired in five spectral bands with ten channels (because of dual polarization) in the wavelength region between 0.8 to 6 cm. The spatial resolution will again be modest and near 25 km for the shortest wavelength.

Future missions are being considered that will attempt improvements in spatial, temporal and spectral resolution. These missions include low-orbiting satellites with modular capability for including new instrumentation. This low-orbiting satellite series will be called Earth Observatory Satellites (EOS). Spatial resolutions in the visible region of the spectrum may be as high as 10 m. Larger observational swath widths would increase the frequency of coverage to 6–9 d with accompanying spatial resolutions 100 m or better. Attention will be given to the possibility of using synthetic aperture radar for providing high spatial resolution in the microwave wavelengths from 1–25 cm.

For snow and ice coverage, the next most interesting spacecraft concept beyond EOS would be the Space Shuttle Sortie-Spacelab concept with polar orbit capability being considered for the 1980's. On the Spacelab, larger instruments of a developmental nature requiring more power, or operation and attendance by a scientist or technician, can be operated and tested for eventual long-term operation. For example large antennae associated with active or passive microwave systems could be tested. Relatively complex visible and infrared spectrometric equipment could also be developed in the Spacelab environments.

Another key facet of future spacecraft systems involves the development of data processing and analysis facilities that would handle data magnitudes as high as 250 megabits per second (Mb/s). It is clear that these data must in the future be optimally processed and delivered to user agencies so that these data products can be applied to resource management problems. To meet these general goals it is imperative that improved data-processing facilities be developed and communications improved between the developers of improved data-processing and dissemination facilities and the potential users of such information. Substantial efforts along these lines are being implemented within NASA in cooperation with major state and federal agencies.

REFERENCES

- Barnes, J. C., and Bowley, C. J. 1968. Snow cover distribution as mapped from satellite photography. *Water Resources Research*, Vol. 4, No. 2, p. 257-71.
- Campbell, W. J., and others. 1974. Dynamics and morphology of Beaufort Sea ice determined from satellites, aircraft, and drifting stations, by W. J. Campbell, P. Gloersen, W. Nordberg and T. T. Wilheit. (In Bock, P., and others, ed. *COSPAR. Approaches to Earth survey problems through use of space techniques. Proceedings of the symposium held in Constance, F.R.G., 23-25 May 1973*. Edited by P. Bock, with the assistance of F. W. G. Baker and S. Ruttenberg. Berlin, Akademie-Verlag, p. 311-27.)
- Campbell, W. J., and others. 1975. Geophysical studies of floating ice by remote sensing, by W. J. Campbell, W. F. Weeks, R. O. Ramseier and P. Gloersen. *Journal of Glaciology*, Vol. 15, No. 73, p. 305-28.
- Chang, T. C., and Gloersen, P. Unpublished. Microwave emissivities of snow fields and glaciers.
- Edgerton, A. T., and others. 1971. *Microwave radiometric investigations of snowpack*, by A. T. Edgerton, A. Strogryn and G. Poe. El Monte, California, Aerojet-General Corp., Microwave Division. (Final report 1285 R-4 for U.S. Geological Survey contract No. 14-08-001-11828.)
- Freden, S. C., and others, ed. 1973. *Symposium on significant results obtained from the Earth Resources Technology Satellite-1. Vol. 1: technical presentations, section A-B. The proceedings of a symposium held by Goddard Space Flight Center at New Carrollton, Maryland, on March 5-9, 1973. Compiled and edited by S. C. Freden, E. P. Mercanti and M.A. Becker*. Washington, D.C., National Aeronautics and Space Administration. Scientific and Technical Information Office. (NASA SP-327.) [Available from the U.S. Government Printing Office, Stock No. 3300-00515.]
- Gloersen, P., and others. 1973[a]. Microwave signatures of first-year and multiyear sea ice, [by] P. Gloersen, W. Nordberg, T. J. Schumgge and T. T. Wilheit [and] W. J. Campbell. *Journal of Geophysical Research*, Vol. 78, No. 18, p. 3564-72.
- Gloersen, P., and others. 1973[b]. *Polar sea ice observations by means of microwave radiometry*, [by] P. Gloersen, T. C. Chang, T. T. Wilheit, W. J. Campbell. Greenbelt, Maryland, Goddard Space Flight Center. (NASA X-652-73-341.) [Also published in *Bulletin of the American Meteorological Society*, Vol. 55, No. 12, 1974, p. 1442-48.]
- Gloersen, P., and others. 1974. Variation of ice morphology of selected mesoscale test areas during the Bering Sea experiment, [by] P. Gloersen, R. [O.] Ramseier, W. J. Campbell, T. C. Chang, T. T. Wilheit. (In *Results of the U.S. contribution to the joint U.S./U.S.S.R. Bering Sea experiment*. Greenbelt, Maryland, Goddard Space Flight Center, p. 75-102. (NASA-X-910-74-141.)
- McClain, E. P., and Baker, D. R. 1969. *Experimental large scale mapping with composite minimum brightness charts*. Washington, D.C., National Oceanic and Atmospheric Administration. (National Environmental Satellite Service Technical Memorandum, NESL TM-12.)
- Salomonson, V. V., and Greaves, J. R. 1974. Advanced ERTS-1 technology for water and marine resources. *Journal of Environmental Sciences*, Vol. 17, No. 2, p. 35-42.
- Salomonson, V. V., and MacLeod, N. H. 1972. Nimbus hydrological observations over the watersheds of the Niger and Indus rivers. (In *4th annual earth resources program review. Vol. 5. . . . Presented at the Manned Spacecraft Center, Houston, Texas, January 17 to 21, 1972*. Houston, Texas, NASA Manned Spacecraft Center, p. 5-1-5-11.)
- Wilheit, T. T., and others. 1973. *Meteorological interpretations of the images from Nimbus 5 electrically scanned microwave radiometer*, [by] T. T. Wilheit, J. Theon, W. Shenk, L. Allison. Greenbelt, Maryland, Goddard Space Flight Center. (NASA X-651-73-189.)

DISCUSSION

A. O. POULIN: It is difficult to obtain the true temperature of the polar surface by infrared means, chiefly because of the inversions. This should have a significant influence on the emissivity results obtained by the ratio of the microwave radiance to the thermal radiance. Also because of the inversion, it is not uncommon that the surface temperature of the Greenland ice sheet increases with altitude, thus confusing the interpretation of the ratio.

P. GLOERSEN: The particular examples chosen appeared to be relatively free of clouds, and are therefore deemed to have reasonably true surface temperatures as obtained from the 10 μ m radiometer (THIR). As more of these examples are processed, of course, confidence in the emissivity contours will be increased if the contours indeed remain stationary.

M. DUNBAR: I understand that in the microwave imagery the cold blue tones are related to multi-year ice. If so why, in the July image, did the Baffin Bay pack appear blue? The ice in this area is always predominantly first-year.

GLOERSEN: This indicates that the first-year ice concentration is less than 100% in that area. Large variations in the ice concentration have been discovered within a season in Hudson Bay, Bering Sea, and many other locales by using Nimbus-5 ESMR.

W. AMBACH: What argument do you have to say that the coastal zone of the Greenland ice sheet is covered by wet snow on the microwave picture taken in July? Could it also be old glacier ice?

GLOERSEN: Yes, it could. In fact this very alternative is predicted by the model I presented yesterday. This can be (but was not, in the example) sorted out by watching the time dependence of the signature, either by day/night orbit comparisons or by watching the development of the signature at the end of the freezing season.

M. F. MEIER: One must remember that the temperature of snow is, in general, a function of depth; thus it is difficult to define a microwave emissivity for this case. The whole concept of interpreting apparent "emissivity" variations is therefore very complex.

GLOERSEN: Quite true; indeed the temperature at ten metres depth is generally regarded as being independent of seasonal variations at the surface in polar regions. At 1.55 cm wavelength, the optical depth is at most 1.5 m (with no volume scattering) but more likely 10–20 cm. Thus the surface temperature will reasonably approximate the properly averaged temperature appropriate for determining the emissivity. The lower the brightness temperature compared to the physical temperature, the better this approximation holds, since this would indicate an increase in the extinction coefficient and hence a reduction of the optical depth.

W. F. WEEKS: A. J. Gow has investigated the increase in grain size with depth at a number of sites in Greenland and Antarctica and has found that these changes are quite systematic and can be predicted if the 10 m temperature and the mean annual accumulation is known. What I do not remember is whether there is a systematic geographic variation in the initial grain size at the surface. If there is, Gow's work could be used to provide the "ground truth" necessary to evaluate your suggestion of a grain-size control of the microwave signatures of Greenland and the Antarctic.

GLOERSEN: S. J. Mock has attempted correlation of such a combination parameter (i.e. the annual accumulation and the 10 m temperature) with the ESMR image of Greenland with only limited success, possibly because the shape of the parameter contours are not well enough known. Also, the surface physical temperatures were not factored into the comparison. Work should continue in making such comparisons with more detailed field data.

M. DE QUERVAIN: In the central part of the ice sheet (*c.* lat. 70° N. and above about 1 800 m) annual stratification is observed. Summer deposits reach grain sizes of *c.* 1–3 mm towards the end of summer season. Winter deposits stay below *c.* 1 mm. (This is a simplified statement.) The depth of the annual period is of the order of 50 to 150 cm according to the region. The actual state of the uppermost layer depends on the recent snowfall history. Between new-snow crystals and rounded grains of 0.3 to 1 mm diameter all intermediate stages may be found.

In the ablation zone conditions are more complex. Melt metamorphism produces snow crystals (temporarily wet) of 1 to 2 mm diameter. But formation of superimposed ice is connected with other crystal features. Ice layers of increasing thickness (cm to dm and m) become dominant toward the coast.

GLOERSEN: It would be indeed worthwhile to obtain iso-crystal-radius contour maps of Greenland and Antarctica for a number of discrete layers down to, say, 3 m depth, for purposes of comparing with the microwave signatures.

C. W. M. SWITHINBANK: One way to try to understand the brightness temperature patterns on the Greenland and Antarctic ice sheets would be to study the stability of the patterns through different seasons of the year.

GLOERSEN: Quite so; this has been done. The patterns persist through the seasons, but the average brightness temperatures rise and fall along with the surface temperatures. Although it is cumbersome, we plan to prepare iso-emissivity contour maps for times other than those shown in the paper. We will be in a better position to do this when multi-spectral microwave data become available.